eIF3 promotes early translation elongation to ensure mitochondrial homeostasis and skeletal muscle health

Yingying Lin [1†], Fajin Li [2,3†], Linlu Huang [1], Haoran Duan [1], Jianhuo Fang [2], Li Sun[1], Xudong Xing [2,3], Guiyou Tian [1], Yabin Cheng [1], Xuerui Yang [2*], Dieter A. Wolf [1*]

[1] School of Pharmaceutical Sciences, Fujian Provincial Key Laboratory of Innovative Drug Target Research & Innovation Center for Cell Stress Signaling, Xiamen University, Xiamen, China
[2] MOE Key Laboratory of Bioinformatics, Center for Synthetic & Systems Biology, School of Life Sciences, Tsinghua University, Beijing, China
[3] Joint Graduate Program of Peking-Tsinghua-National Institute of Biological Science, Tsinghua University, Beijing 100084, China

* Corresponding authors
† Equal contributions

Address for correspondence:

Dieter A. Wolf, M.D.
School of Pharmaceutical Sciences
Xiamen University
Xiamen, China

+86 136 009 45744
dwolf@xmu.edu.cn

Abstract

eIF3 is a multi-subunit complex with numerous functions in canonical translation initiation, including mRNA recruitment to the 40S ribosome, scanning for the start codon, and inhibition of premature 60S subunit joining [1–3]. eIF3 was also found to interact with 40S and 60S ribosomal proteins and translation elongation factors [4], but a direct involvement in translation elongation has never been demonstrated. Using ribosome profiling, we found that eIF3 deficiency reduced early ribosomal elongation speed between codons 25 and 75 on a set of ~2,700 mRNAs encoding proteins associated with mitochondrial and membrane functions, resulting in defective synthesis of their encoded proteins. To promote early elongation, eIF3 forms stable protein interactions with 80S ribosomes translating the first ~60 codons and serves as a platform to recruit protein quality control factors, functions required for normal mitochondrial physiology. Accordingly, eIF3e$^{+/-}$ knockout mice accumulate defective mitochondria in skeletal muscle and show a progressive decline in muscle strength with age. Hence, in addition to its canonical role in translation initiation, eIF3 interacts with 80S ribosomes to enhance, at the level of early elongation, the synthesis of proteins with membrane-associated functions, an activity that is critical for mitochondrial physiology and muscle health.

Introduction

The interaction of the 13 subunit eIF3 complex with mRNA is central to all forms of translation initiation, including cap-dependent and cap-independent mechanisms [5–7]. eIF3 promotes ternary complex recruitment, binding of the 43S pre-initiation complex to mRNA, as well as scanning processivity and fidelity [1,2]. Although eIF3 has traditionally been thought to be released from ribosomes upon 40S-60S subunit joining in vitro [8], recent evidence in yeast

suggested that it can remain associated with 80S ribosomes during translation of short uORFs in order to facilitate re-initiation on downstream ORFs [9]. In addition, pull-down experiments indicated that yeast eIF3 forms stable in vivo interactions with factors involved in translation elongation (40S and 60S ribosomal proteins, eukaryotic elongation factors (eEFs), and tRNA synthetases), suggesting an unexplored role in integrating translation initiation with elongation [4].

Results

To explore the global role of eIF3 in mRNA translation at nucleotide resolution, we performed ribosome profiling [10] in MCF-10A cells upon knockdown (KD) of eIF3 subunit "e", a treatment that resulted in the depletion of eIF3e without destroying the eIF3 holo-complex (Extended Data Fig. 1). Highly reproducible triplicate experiments (Extended Data Fig. 2) revealed several hundred significant changes in translational efficiency (TE) (Fig. 1a, Supplementary Data File 1). The group of 220 mRNAs with increased TE was enriched for mitochondrial and transmembrane proteins, in addition to proteins functioning in mRNA translation (Fig. 1a). Conversely, TE was decreased for a group of 240 proteins that was enriched in cell adhesion, mRNA processing and metabolic functions (Fig. 1a).

Increased TE for mRNAs encoding mitochondrial proteins in eIF3e-KD cells contradicted our previous demonstration in fission yeast that eIF3e promotes the synthesis of mitochondrial proteins [11]. Consistent with the previous data, quantitative proteomics by pulsed SILAC (pSILAC) [12] confirmed decreased synthesis of mitochondrial and transmembrane proteins in eIF3e-KD cells (Fig. 1b, Supplementary Data File 2). In contrast, the synthesis of proteins involved in glucose metabolism, ribosome biogenesis, tRNA aminoacylation, and protein folding was increased (Fig. 1b), suggesting that eIF3e-KD cells attempt to boost protein synthesis and folding capacity. However, most proteins encoded by mRNAs with increased TE

for which pSILAC data were obtained (a total of 49) showed either reduced or largely unchanged synthesis (Fig. 1c, Supplementary Data File 3). Thus, eIF3e-KD appears to result in reduced synthesis of mitochondrial and transmembrane proteins despite paradoxical increases in the apparent TEs of their encoding mRNAs.

Reconciling this paradox, we found in a meta-analysis of normalized ribosome densities a pronounced accumulation of ribosomes in a region between codons 25 and 75 in eIF3e-KD cells with a distinct peak at codon 50 (Extended Data Fig. 3a). No such accumulation was seen surrounding the stop codon or in the total RNA samples (Extended Data Fig. 3a,b). From a total dataset of 19330 mRNAs, we identified 2683 mRNAs with a >2-fold increase in ribosome density between codons 25 and 75 (Fig. 2a, Extended Data Fig. 3c, Supplementary Data File 4). This increase was reflected in a highly significant 5' shift in global ribosome positioning along mRNAs (Fig. 2b). Selective ribosome accumulation in the region encompassing codon 50 was also apparent at the level of specific mRNAs (Fig. 2c, Extended Data Fig. 3d). This data suggested that, due to abnormal localized ribosome accumulation, global ribosome occupancy in eIF3e deficient cells is not a surrogate of protein synthesis and, in fact, shows an inverse relationship with apparent TE (Fig. 1c). Most mRNAs for which disruption of eIF3 increased early ribosome density were impaired in translational efficiency as indicated by reduced synthesis of their encoded proteins (Fig. 2d, Supplementary Data File 5). Thus, loss of eIF3 integrity causes a slowdown in early translation elongation resulting in localized ribosome accumulation between codons 25 – 75.

The set of 2683 mRNAs that depended on eIF3e for elongation showed strong enrichment of functional pathways which were dominated by RNA metabolism, protein homeostasis, and membrane-associated processes (Fig. 2e, Supplementary Data File 6). This

encompassed hundreds of mitochondrial proteins, including subunits of respiration complexes I, IV, and V. Whereas there were no common RNA or amino acid sequence motifs apparent in this group of mRNAs that might underly their dependence on eIF3 for early translation elongation, their encoded proteins have increased hydrophobicity and positive charge within the N-terminal ~25 residues (Fig. 2f,g), which are well-established characteristics of mitochondrial targeting sequences [13]. eIF3-dependent mRNAs also had a lower tRNA adaptation index in the region encoding the N-terminal ~40 amino acids (Fig. 2h), suggesting that these mRNAs begin their translation at a slower pace than eIF3-independent mRNAs, a feature known to be important for efficient synthesis of membrane proteins [14].

To mechanistically address the function of eIF3 in elongation, we asked whether the initiation factor physically interacts with elongating 80S ribosomes. On sucrose density gradients, eIF3 subunits were strongly enriched in 40S monosomal fractions but also co-eluted with polysomes (Fig. 3a), suggesting association with actively translating 80S ribosomes. Unlike the ribosomal proteins RPL7 and RPS19, eIF3 subunits did not increase proportionally with the density of the polysomal fractions (Fig. 3a), indicating that eIF3 associates with only a subset of 80S ribosomes. To exclude that eIF3 co-elution with polysomes was due to the presence of scanning 43S pre-initiation complexes on polysomal mRNAs, we digested polysomal fractions with RNAse I and purified the resulting 80S ribosomal complexes by sucrose density gradient fractionation. LC-MS/MS revealed copious amounts of eIF3 in addition to 40S and 60S ribosomal proteins in purified 80S complexes (Fig. 3b, Supplementary Data File 7). Purified 80S complexes also contained other proteins we had previously found to interact with eIF3, including elongation factors (eEFs) and the 26S proteasome [4]. Quantitative proteomics of 80S fractions obtained upon knockdown of eIF3e revealed a decrease in the abundance of protein quality

control factors including chaperones, the CCT/TRiC chaperonin, and the proteasome despite increased amounts of ribosomal proteins (Fig. 3c, Supplementary Data File 8). This depletion suggests that eIF3, via its eIF3e subunit, serves to recruit protein quality control factors to 80S ribosomes in order to promote translation elongation.

To map the location of eIF3-associated 80S ribosomes on mRNA, we performed selective ribosome profiling [15]. Following digestion of MCF-10A cell lysate with RNAse I, eIF3-associated ribosomes were immunopurified using eIF3b antibodies which efficiently precipitate the eIF3 complex (Extended Data Fig. 1), and ribosome protected fragments (RPFs) were extracted from the immunopurified eIF3-80S complexes for sequencing (Extended Data Fig. 4a). Enrichment analysis of the eIF3-bound RPFs relative to total RPFs was used to map the presence of eIF3-associated 80S ribosomes on mRNA. The analysis revealed a consistent enrichment of eIF3-80S complexes within the first ~60 codons on the group of 2683 mRNAs identified by ribosome profiling as being dependent on eIF3e for efficient translation elongation (Fig. 3d). An unbiased search for mRNAs displaying enrichment of eIF3 on 80S ribosomes in the 5' part of the coding region identified a class of 2543 transcripts (Fig. 3e, Supplementary Data File 9), which showed a highly significant overlap with the set of 2683 eIF3-dependent mRNAs (Extended Data Fig. 4b). This set was enriched for the same functional categories, dominated by mitochondrial proteins and membrane-associated processes (Fig. 3f, Supplementary Data File 10).

Reflecting the functional pathway enrichment, eIF3e-KD cells showed a marked disturbance in organelle structure with accumulation of electron sparse vesicles that were filled with multilamellar membranous contents, morphological features consistent with lysosomes (Fig. 4a). To decipher the identity of the vesicles accumulating in eIF3e-KD cells, we used

transfection of a mCherry-EGFP-LC3B fusion protein as an autophagosomal/lysosomal marker. In si-Control cells, mCherry single positive and mCherry-EGFP double positive yellow vesicles coexisted at relatively low numbers, indicating intact autophagosomal and lysosomal compartments (Fig. 4b, Extended Data Fig. 5d). Upon the addition of the lysosomal inhibitor bafilomycin A1, more yellow puncta were observed, a finding that is consistent with inhibition of lysosomal degradation at constant autophagic flux (Fig. 4b, Extended Data Fig. 5d). In eIF3e-KD cells, the majority of puncta appeared red, but yellow puncta were observed upon treatment with bafilomycin A. This indicates intact autophagic flux but increased lysosomal load in eIF3e-depleted cells, possibly to clear defective mitochondria. Supporting this idea, mitochondrial cristae appeared dilated with fuzzy borders in eIF3e-KD cells (Fig. 4a), which also showed decreased mitochondrial respiration (Fig. 4c).

A phenotype indicative of mitochondrial dysfunction was also observed in skeletal muscle of heterozygous eIF3e$^{+/-}$ knockout mice we created. Muscle of 10 to 18 week old eIF3e$^{+/-}$ mice showed a pronounced accumulation of hyperfused intramyofibrillar mitochondria (Fig. 4d, e, Extended Data Fig. 6c), ostensibly an adaptive response to energy stress caused by eIF3 deficiency [16]. In addition, severe ultrastructural damage to the sarcomers with degeneration of the contractile elements reminiscent of mitochondrial myopathy [17] was observed (Fig. 4e, Extended Data Fig 6c). Significant impairment of neuromuscular function was indicated by a progressive reduction in grip strength of male and female eIF3e$^{+/-}$ mice beginning at 2 months of age (Fig. 4f).

Discussion

Our findings suggest a revised model for eIF3 function that integrates roles in translation initiation with elongation and quality control (Fig. 4g). Instead of being immediately released

during 40S-60S subunit joining, eIF3 initially remains on the elongating 80S ribosome. eIF3 is known to undergo conformational changes during the initiation reaction [18,19] that are consistent with persistence on the 80S ribosome. The majority of ribosomes subsequently loose eIF3 within the first few codons, but eIF3 stays on the ribosome for up to ~60 codons on a large set of mRNAs encoding proteins with membrane-associated functions. Similar to mechanisms thought to govern SRP pre-recruitment to ribosomes even before the emergence of signal sequences [21] , the trigger for early loss versus prolonged retention of eIF3 may be controlled by the nascent chain from within the ribosome exit tunnel [22] or by features of the 3'-UTRs [21]. It is also possible that early translation speed determines eIF3 retention, with mRNAs having suboptimal early codons retaining eIF3 longer. During slow initial progression of 80S ribosomes, eIF3, via its eIF3e subunit, may serve as platform for the recruitment of chaperones and quality control factors that ensure correct targeting of nascent proteins to their subcellular destinations, including the endoplasmic reticulum membrane for further sorting into the endosomal and secretory pathways as well as the mitochondrial retrieval pathway [20]. If eIF3 activity is impaired, membrane-associated processes including mitochondrial function and dynamics are disturbed, resulting in a profound impact on cellular physiology and organismal health.

References and Notes:

1. Valášek, L. S. *et al.* Embraced by eIF3: structural and functional insights into the roles of eIF3 across the translation cycle. *Nucleic Acids Res* **45**, 10948–10968 (2017).
2. Hinnebusch, A. G. Structural Insights into the Mechanism of Scanning and Start Codon Recognition in Eukaryotic Translation Initiation. *Trends in Biochemical Sciences* **42**, 589–611 (2017).
3. Cate, J. H. D. Human eIF3: from 'blobology' to biological insight. *Phil. Trans. R. Soc. B* **372**, 20160176 (2017).
4. Sha, Z. *et al.* The eIF3 Interactome Reveals the Translasome, a Supercomplex Linking Protein Synthesis and Degradation Machineries. *Molecular Cell* **36**, 141–152 (2009).
5. Lee, A. S. Y., Kranzusch, P. J. & Cate, J. H. D. eIF3 targets cell-proliferation messenger RNAs for translational activation or repression. *Nature* **522**, 111–114 (2015).
6. Lee, A. S. Y., Kranzusch, P. J., Doudna, J. A. & Cate, J. H. D. eIF3d is an mRNA cap-binding protein that is required for specialized translation initiation. *Nature* **536**, 96–99 (2016).
7. Wolf, D. A., Lin, Y., Duan, H. & Cheng, Y. eIF-Three to Tango: Emerging Functions of Translation Initiation Factor eIF3 in Protein Synthesis and Disease. *Journal of Molecular Cell Biology*
8. Peterson, D. T., Merrick, W. C. & Safer, B. Binding and release of radiolabeled eukaryotic initiation factors 2 and 3 during 80 S initiation complex formation. *J. Biol. Chem.* **254**, 2509–2516 (1979).

9. Mohammad, M. P., Munzarová Pondělíčková, V., Zeman, J., Gunišová, S. & Valášek, L. S. In vivo evidence that eIF3 stays bound to ribosomes elongating and terminating on short upstream ORFs to promote reinitiation. *Nucl Acids Res* **45**, 2658–2674 (2017).
10. Ingolia, N. T., Ghaemmaghami, S., Newman, J. R. S. & Weissman, J. S. Genome-Wide Analysis in Vivo of Translation with Nucleotide Resolution Using Ribosome Profiling. *Science* **324**, 218–223 (2009).
11. Shah, M. *et al.* A Transcript-Specific eIF3 Complex Mediates Global Translational Control of Energy Metabolism. *Cell Reports* **16**, 1891–1902 (2016).
12. Schwanhäusser, B., Gossen, M., Dittmar, G. & Selbach, M. Global analysis of cellular protein translation by pulsed SILAC. *Proteomics* **9**, 205–209 (2009).
13. Omura, T. Mitochondria-Targeting Sequence, a Multi-Role Sorting Sequence Recognized at All Steps of Protein Import into Mitochondria. *J Biochem (Tokyo)* **123**, 1010–1016 (1998).
14. Acosta-Sampson, L. *et al.* Role for ribosome-associated complex and stress-seventy subfamily B (RAC-Ssb) in integral membrane protein translation. *J. Biol. Chem.* **292**, 19610–19627 (2017).
15. Becker, A. H., Oh, E., Weissman, J. S., Kramer, G. & Bukau, B. Selective ribosome profiling as a tool for studying the interaction of chaperones and targeting factors with nascent polypeptide chains and ribosomes. *Nature Protocols* **8**, 2212–2239 (2013).
16. Tondera, D. *et al.* SLP-2 is required for stress-induced mitochondrial hyperfusion. *The EMBO Journal* **28**, 1589–1600 (2009).
17. Vogel, H. Mitochondrial Myopathies and the Role of the Pathologist in the Molecular Era. *Journal of Neuropathology & Experimental Neurology* **60**, 217–227 (2001).

18. Eliseev, B. *et al.* Structure of a human cap-dependent 48S translation pre-initiation complex. *Nucleic Acids Res* **46**, 2678–2689 (2018).

19. Simonetti, A. *et al.* eIF3 Peripheral Subunits Rearrangement after mRNA Binding and Start-Codon Recognition. *Molecular Cell* **63**, 206–217 (2016).

20. Hansen, K. G. *et al.* An ER surface retrieval pathway safeguards the import of mitochondrial membrane proteins in yeast. *Science* **361**, 1118–1122 (2018).

21. Chartron, J. W., Hunt, K. C. L. & Frydman, J. Cotranslational signal-independent SRP preloading during membrane targeting. *Nature* **536**, 224–228 (2016).

22. Berndt, U., Oellerer, S., Zhang, Y., Johnson, A. E. & Rospert, S. A signal-anchor sequence stimulates signal recognition particle binding to ribosomes from inside the exit tunnel. *PNAS* **106**, 1398–1403 (2009).

23. Ingolia, N. T., Brar, G. A., Rouskin, S., McGeachy, A. M. & Weissman, J. S. The ribosome profiling strategy for monitoring translation in vivo by deep sequencing of ribosome-protected mRNA fragments. *Nature Protocols* **7**, 1534–1550 (2012).

24. Xiao, Z., Zou, Q., Liu, Y. & Yang, X. Genome-wide assessment of differential translations with ribosome profiling data. *Nature Communications* **7**, 11194 (2016).

25. Dobin, A. *et al.* STAR: ultrafast universal RNA-seq aligner. *Bioinformatics* **29**, 15–21 (2013).

26. Xiao, Z. *et al.* De novo annotation and characterization of the translatome with ribosome profiling data. *Nucleic Acids Res* **46**, e61–e61 (2018).

27. Schuller, A. P., Wu, C. C.-C., Dever, T. E., Buskirk, A. R. & Green, R. eIF5A Functions Globally in Translation Elongation and Termination. *Molecular Cell* **66**, 194-205.e5 (2017).

28. Tuller, T. *et al.* An Evolutionarily Conserved Mechanism for Controlling the Efficiency of Protein Translation. *Cell* **141**, 344–354 (2010).

29. Zhou, Y. *et al.* Metascape provides a biologist-oriented resource for the analysis of systems-level datasets. *Nature Communications* **10**, (2019).

30. Cline, M. S. *et al.* Integration of biological networks and gene expression data using Cytoscape. *Nat Protoc* **2**, 2366–2382 (2007).

Acknowledgments

We thank M. Hansen for the pDest-mCherry-EGFP-LC3B plasmid and all members of the Wolf and Yang labs for discussion. The National Center for Protein Science (Beijing) is thanked for providing MS service for the pSILAC analysis. We also acknowledge the support of the Platforms of Genome Sequencing and High-Performance Computing of the National Protein Science Facility (Beijing) at Tsinghua University. D.A.W.'s lab at Xiamen University is partially funded through grant 81773771 from the National Science Foundation of China and the 1000 Talent Program of the Government of the People's Republic of China. X. Y.'s lab is funded by the National Key Research and Development Program, Precision Medicine Project (2016YFC0906001), the National Natural Science Foundation of China (91540109 and 31671381) and the 1000 Talent Program (Youth Category).

Author contributions

Conceptualization, Y.L. and D.A.W.; Methodology, Y.L., L.H., H.D., G.T., F.L. and X.X.; Formal Analysis, F.L., X.X., X.Y., Y.L.; Investigation, Y.L., F.L., L.H., H.D., L.S., J.F., X.X., G.T.; Writing – Original Draft, D.A.W.; Writing – Review & Editing, Y.L., F.L., L.H., L.S., J.F., H.D., X.X., G.T., Y.C., X.Y., D.A.W.; Visualization, Y.L., F.L. X.Y., D.A.W.; Supervision, Y.C., X.Y., and D.A.W.; Funding Acquisition, Y.C., X.Y., and D.A.W.

Author information

Data are deposited in Gene Expression Omnibus (GSE131074) and Peptide Atlas (PASS01378).

The authors declare no competing interests.

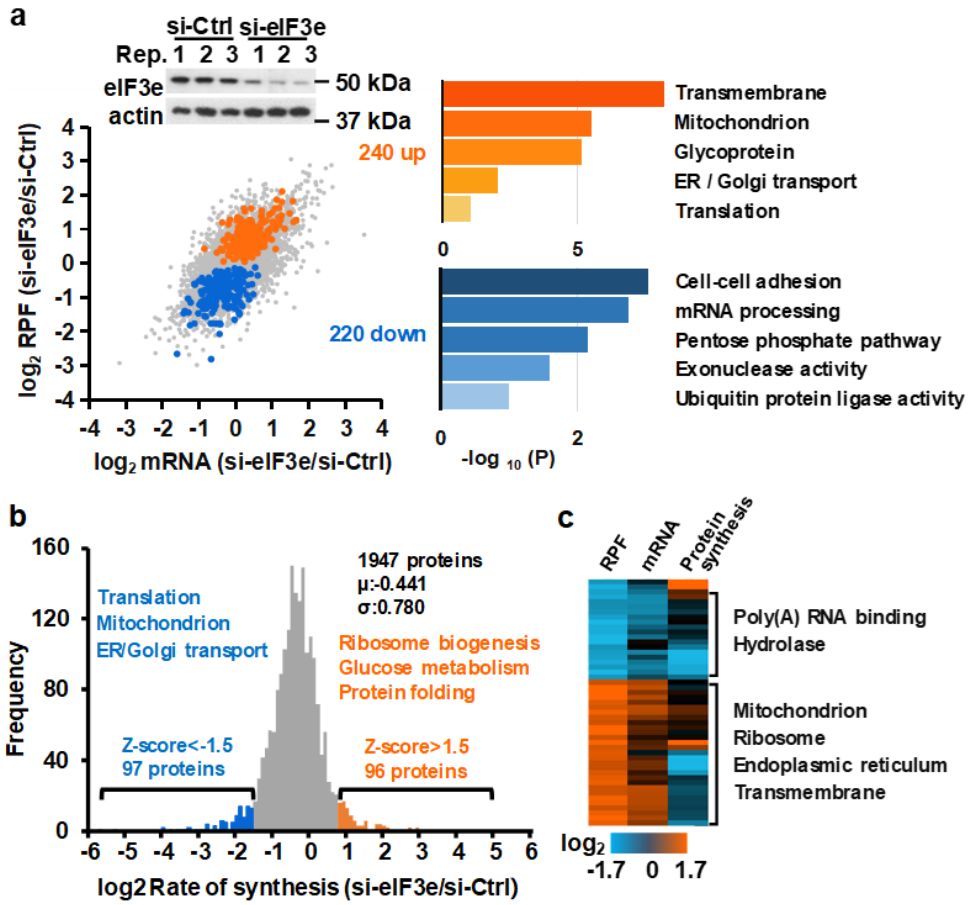

Figure 1 Effect of knockdown of eIF3e on ribosome density and protein synthesis

a) Triplicate ribosome profiling experiments were performed with MCF-10A cells after knockdown of eIF3e for 72 hours. Total mRNA was sequenced in parallel, and log2 si-eIF3e/si-Control changes in mRNA were plotted versus log2 changes in ribosome protected fragments (RPF). The colored datapoint indicate significant changes in RPF ($p < 0.01$) but not in mRNA ($p > 0.01$). The right panel shows enriched functions in the up- and down-regulated groups of mRNAs.

b) Protein synthesis as determined by pulsed SILAC. The graph highlights proteins whose synthesis is either down- or up-regulated upon knockdown of eIF3e.

c) Heatmap comparing of ribosome density (RPF) with mRNA abundance and protein synthesis. Log2 si-eIF3e/si-Control.

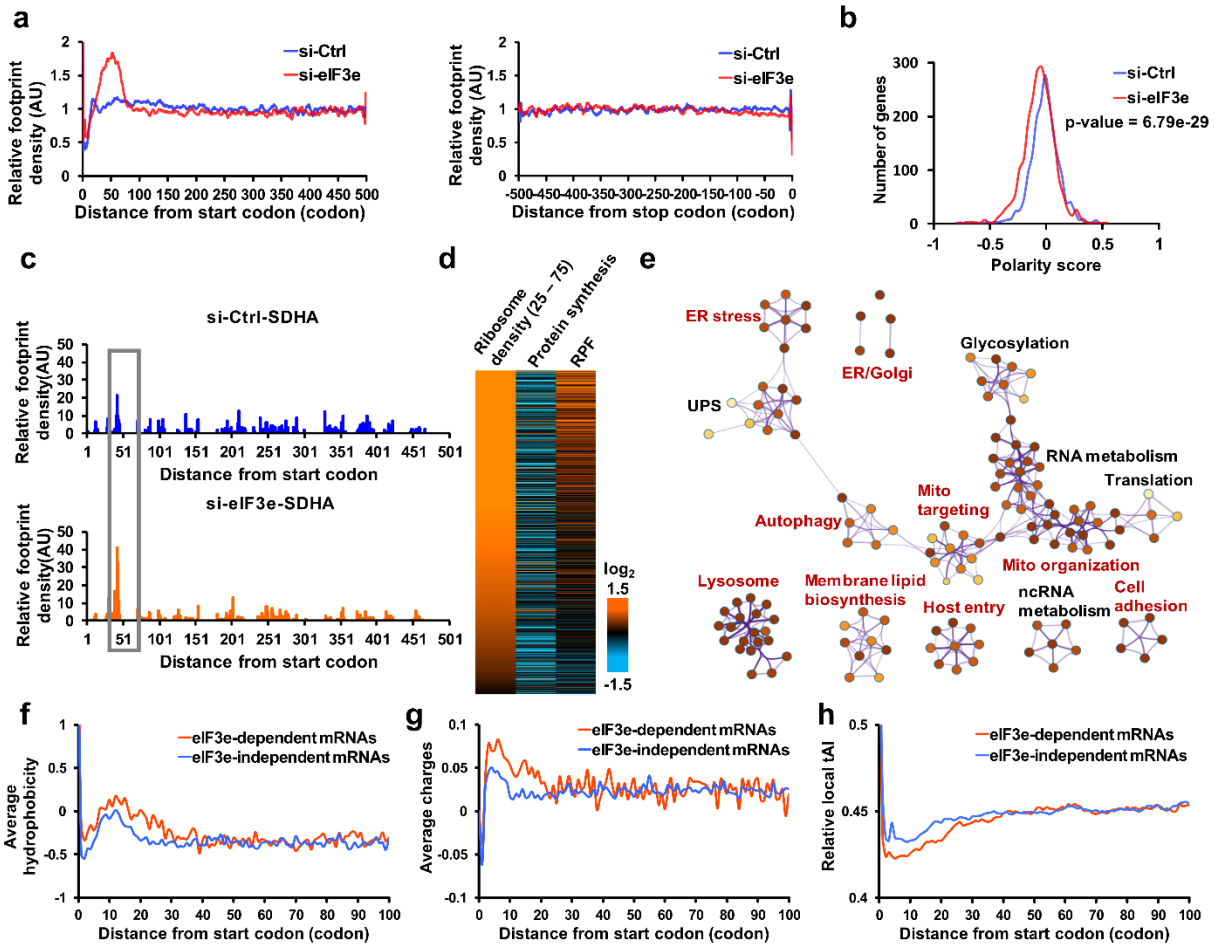

Figure 2 Effect of eIF3 on early translation elongation

a) Meta-analysis of 2683 mRNAs that show a pronounced accumulation of ribosomes in a region between codons 25 – 75. No such accumulation is seen at the stop codon.

b) Global polarity score indicating the relative ribosome distribution towards the 5' (negative score) or 3' (positive score) region of mRNAs.

c) Accumulation of ribosomes in the region between codons 25 and 75 in the mRNA encoding SDHA.

d) Heatmap showing protein synthesis rates and total ribosome densities (RPF) of 1209 mRNAs with >2-fold increased ribosome density between codons 25 – 75.

e) Network of Gene Ontology terms enriched in the set of 2683 mRNAs with increased ribosome density between codons 25 and 75. Clusters denoted in red indicate membrane-associated functions.

f) Average hydrophobicity of the proteins encoded by the 2683 mRNAs that show high ribosome density in eIF3e depleted cells ("eIF3e-dependent mRNAs") versus the proteins encoded by the remaining set of 16229 mRNAs that do not show the elongation block ("eIF3e-independent mRNAs").

g) Average positive charge (lysine and arginine residues) of the protein sets described in f).

h) Relative local tAI of the protein sets described in f).

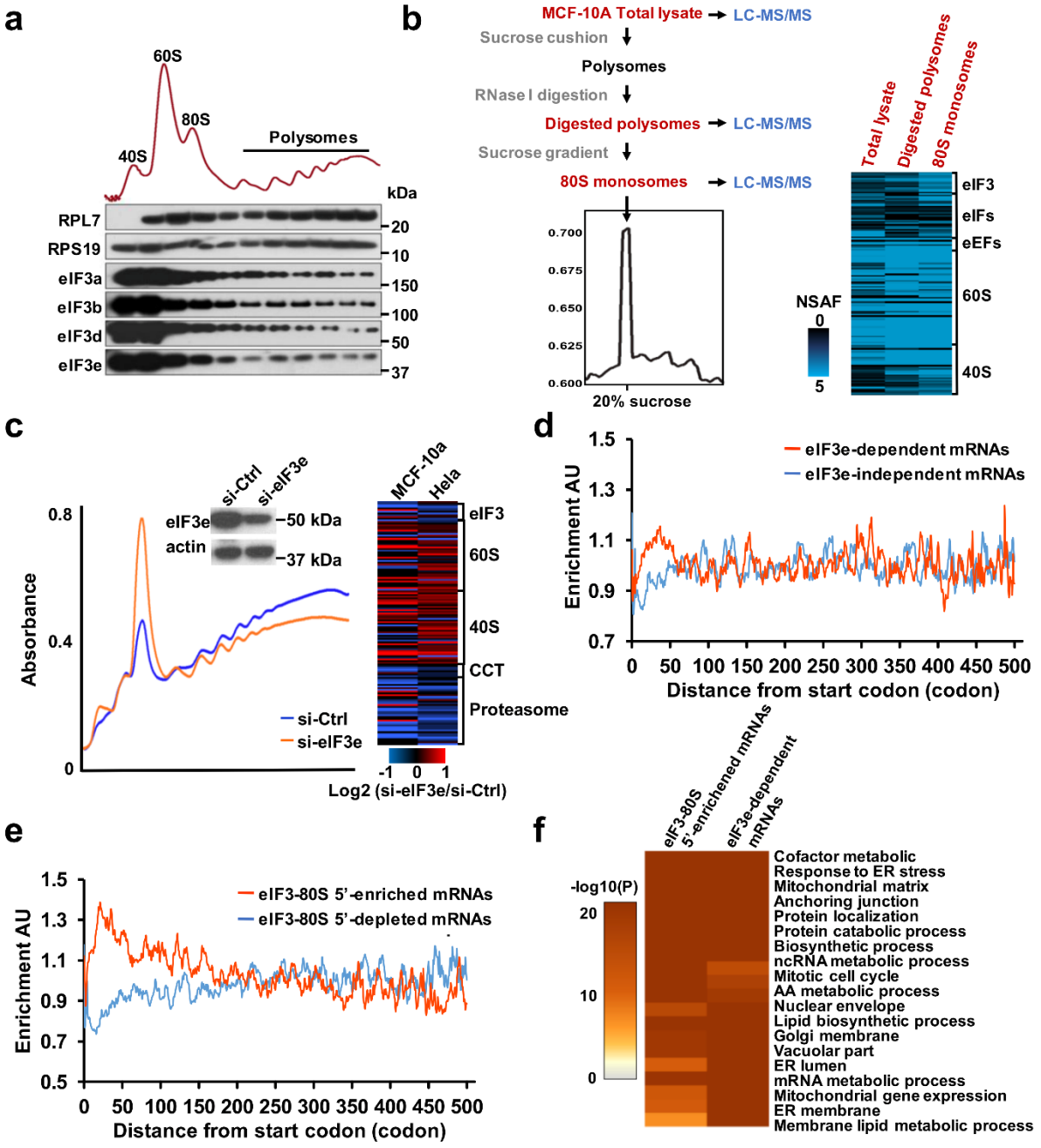

Figure 3 eIF3 associates with 80S ribosomes early during translation

a) Polysome profiling of MCF-10A cells by sucrose density gradient centrifugation. The elution profiles of the indicated translation proteins were determined by immunoblotting.

b) Purification scheme and heatmap showing the abundance of the indicated protein groups in total MCF-10A cell lysate, RNAse I digested polysomes, and purified 80S monosomes as determined by quantitative LC-MS/MS.

c) Lysate of MCF-10A and HeLa cells 72 h after knockdown of eIF3e were separated on sucrose density gradients, followed by quantitative LC-MS/MS. Heatmap shows Log2 changes between si-Control and si-eIF3e cells.

d) Cumulative distribution of eIF3-associated 80S ribosomes on the set of 2683 eIF3e-dependent mRNAs compared to the set of 5320 eIF3e-independent mRNAs as established by selective profiling of eIF3b-associated ribosomes.

e) Distribution of eIF3b-associated 80S ribosomes on a set of 2543 mRNAs showing global 5' accumulation of eIF3b-associated ribosomes relative to all ribosomes (polarity difference <0, "eIF3-80S 5'-enriched mRNAs", see Methods for details). The blue graph represents a reference set of 5204 mRNA with a polarity difference >0 ("eIF3-80S 5'-depleted mRNAs).

f) Overlap in the enrichment of Gene Ontology terms in the set of 2683 eIF3-dependent mRNAs and the set of 2543 mRNAs with increased density of eIF3b-associated ribosomes towards the 5' end ("eIF3-80S 5'-enriched mRNAs").

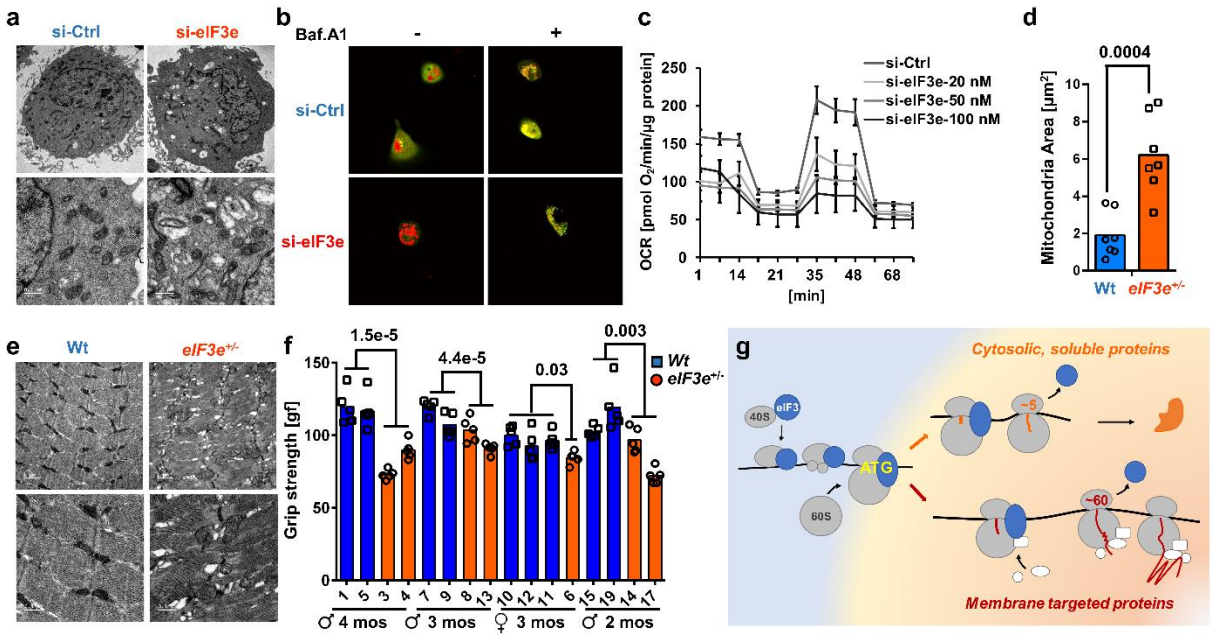

Figure 4 Effect of eIF3e on cell and muscle physiology

a) Transmission electron micrographs on MCF-10A cells upon knockdown of eIF3e for 72 hours. See Extended Data Fig. 4a for eIF3e knockdown efficiency.

b) Live cell imaging of MCF-10A cells transfected with a plasmid driving mCherry-EGFP-LC3B fusion protein. Lysosomes in red, autophagosomes in yellow. See Extended Data Fig. 4b for eIF3e knockdown efficiency.

c) Mitochondrial oxygen consumption rate (OCR) of MCF-10A cells exposed to increasing concentrations of si-eIF3e for 72 hours. OCR was measured in a FX Flux Analyzer. See Extended Data Fig. 4c for eIF3e knockdown efficiency.

d) Electron micrographs of forelimb skeletal muscle from wildtype and eIF3$^{+/-}$ heterozygous knockout mice. See Extended Data Fig. 6 for genotyping.

e) Quantification of mitochondrial area in electron micrographs of skeletal muscle from wildtype (n = 6) and eIF3$^{+/-}$ (n = 6) mice.

f) Grip test to measure muscle strength in wildtype and eIF3$^{+/-}$ heterozygous knockout mice.

g) Model for the role of eIF3 in translation initiation and elongation.

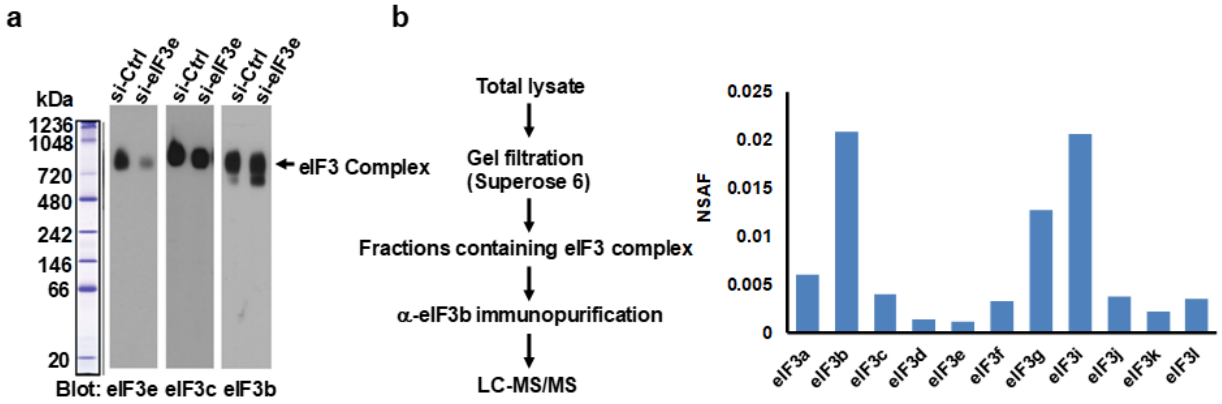

Extended Data Fig. 1 Effect of eIF3e knockdown on eIF3 holo-complex

a) MCF7 cells were transfected with si-eIF3e or si-Control for 72 h, followed by separation of cell lysate by native PAGE and detection of eIF3 by immunoblotting with the indicated antibodies. eIF3e knockdown depletes eIF3e from the ~800 kDa eIF3 complex, but other subunits, including eIF3b and eIF3c as well as the overall size of the complex are maintained.

b) Demonstration that the ~800 kDa complex shown in a) corresponds to the eIF3 holo-complex. MCF7 lysate was separated by gel filtration on a S300 column, and the fractions containing the ~800 kDa complex were pooled and used for immunoprecipitation with eIF3b antibodies or normal rabbit IgG as control. The immunopurified material was analyzed by LC-MS/MS, and eIF3 subunits were quantified using normalized spectral abundance factors (NSAF). The data shows that the ~800 kDa complex contains most eIF3 subunits, although subunits eIF3h and eIF3m were not identified. The IgG negative control did not pull down any eIF3 subunits.

a

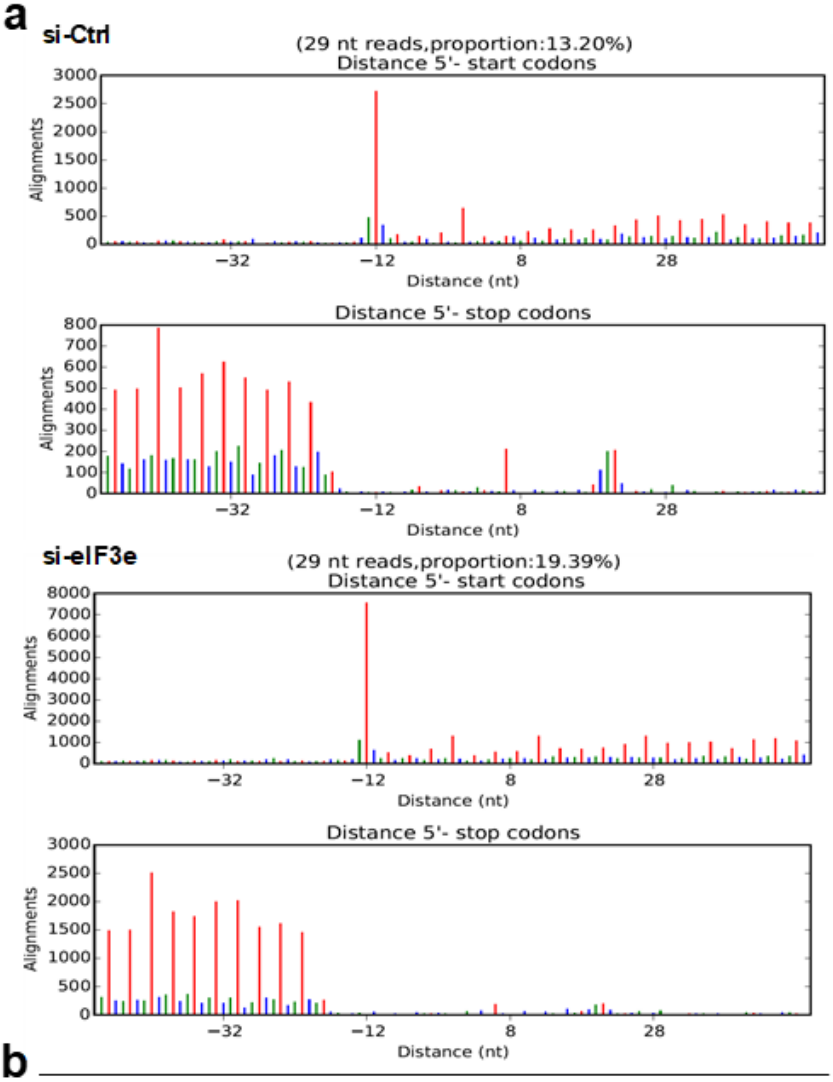

b

Correlation Factor	si-Ctrl_1	si-Ctrl_2	si-Ctrl_3	si-eIF3e_1	si-eIF3e_2	si-eIF3e_3
si-Ctrl_1	1					
si-Ctrl_2	0.996106	1				
si-Ctrl_3	0.973929	0.986551	1			
si-eIF3e_1	0.842613	0.860208	0.896808	1		
si-eIF3e_2	0.837665	0.856165	0.894911	0.998239	1	
si-eIF3e_3	0.855581	0.872628	0.906566	0.998039	0.99748	1

Extended Data Fig. 2 Quality and reproducibility of the ribosome profiling datasets

a) RPF reads derived from si-Control and si-eIF3e samples and mapped to the human transcriptome reveal the 3-nucleotide periodicity typical of ribosome protected fragments.

b) Correlation coefficients for the triplicate datasets obtained from si-Control and si-eIF3e samples.

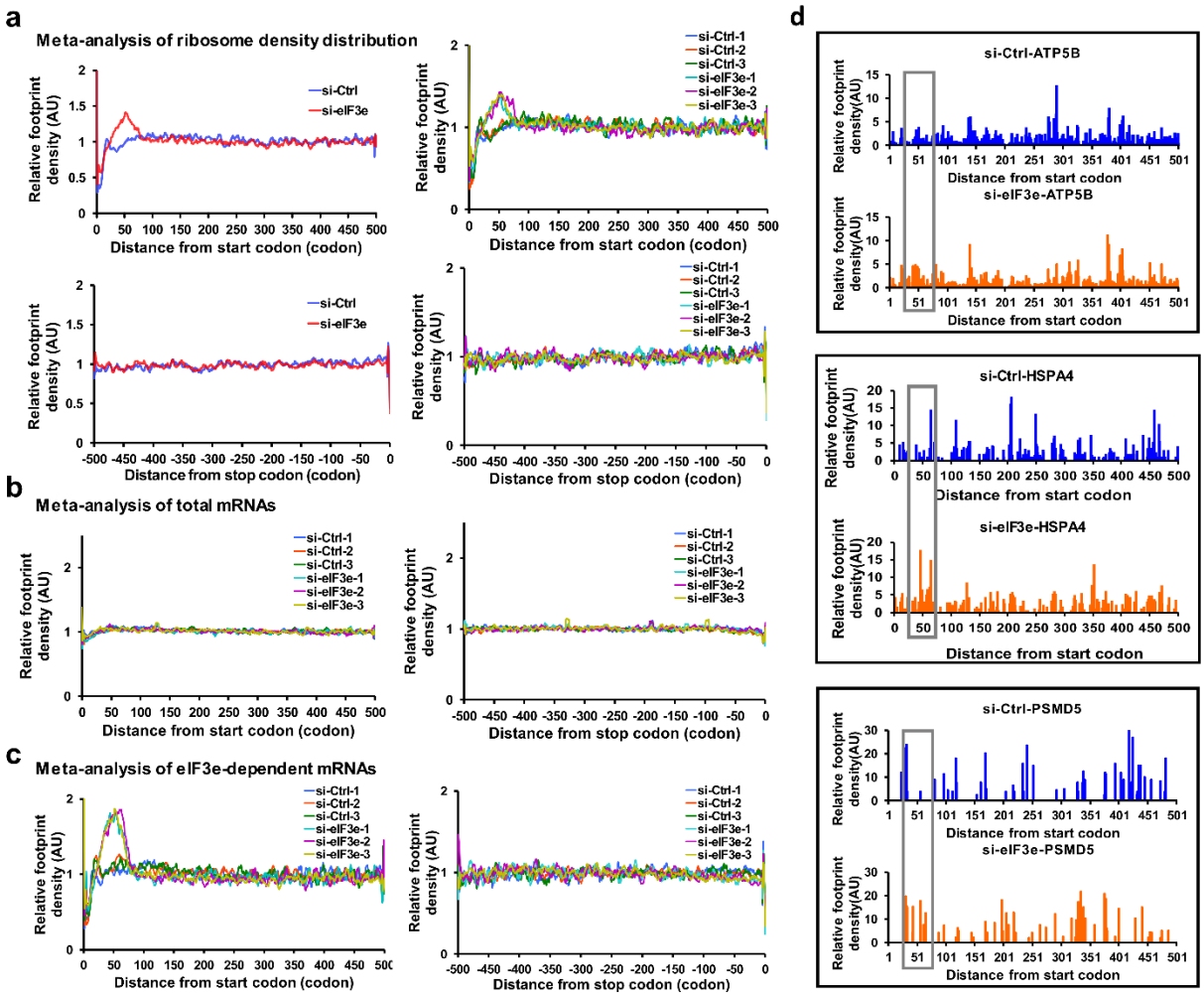

Extended Data Fig. 3 Evidence for ribosomal pausing between codons 25 and 75

a) Meta-analysis of ribosome density distribution for the total datasets after filtering (see Methods for details). The left panel shows averages from triplicate si-Control and si-eIF3e datasets, the right panel shows the three individual datasets. Top panels show the region from the start codon to codon 500, the bottom panel shows the last 500 codons before the stop codon.

b) Same meta-analysis as in a) performed on the total mRNA datasets, which do not show a peak between codons 25 - 75.

c) Meta-analysis of ribosome density distribution for the set of 2683 mRNAs which depend on eIF3e for efficient early translation elongation. Individual replicates are shown for the regions 500 codons downstream of the start codon and upstream of the stop codon.

d) Examples of individual mRNAs displaying selective ribosome accumulation in the region between 25-75 codons.

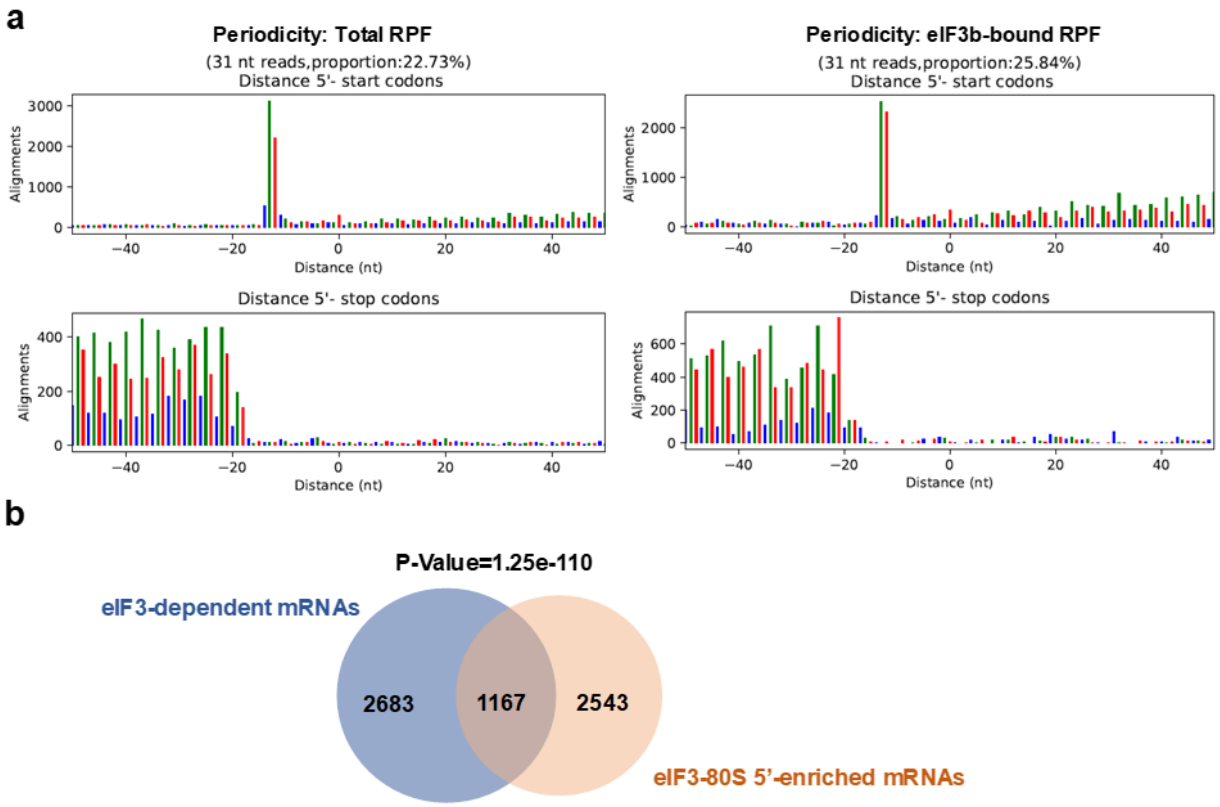

Extended Data Fig. 4 Characteristics of the eF3b selective ribosome profiling dataset

a) 3-nucleotide periodicity of the RPFs derived from all ribosomes and from eIF3b-associated ribosomes.

b) Overlap in the set of 2683 eIF3-dependent mRNAs and the set of 2543 mRNAs with increased density of eIF3b-associated ribosomes ("eIF3-80S 5'-enriched mRNAs").

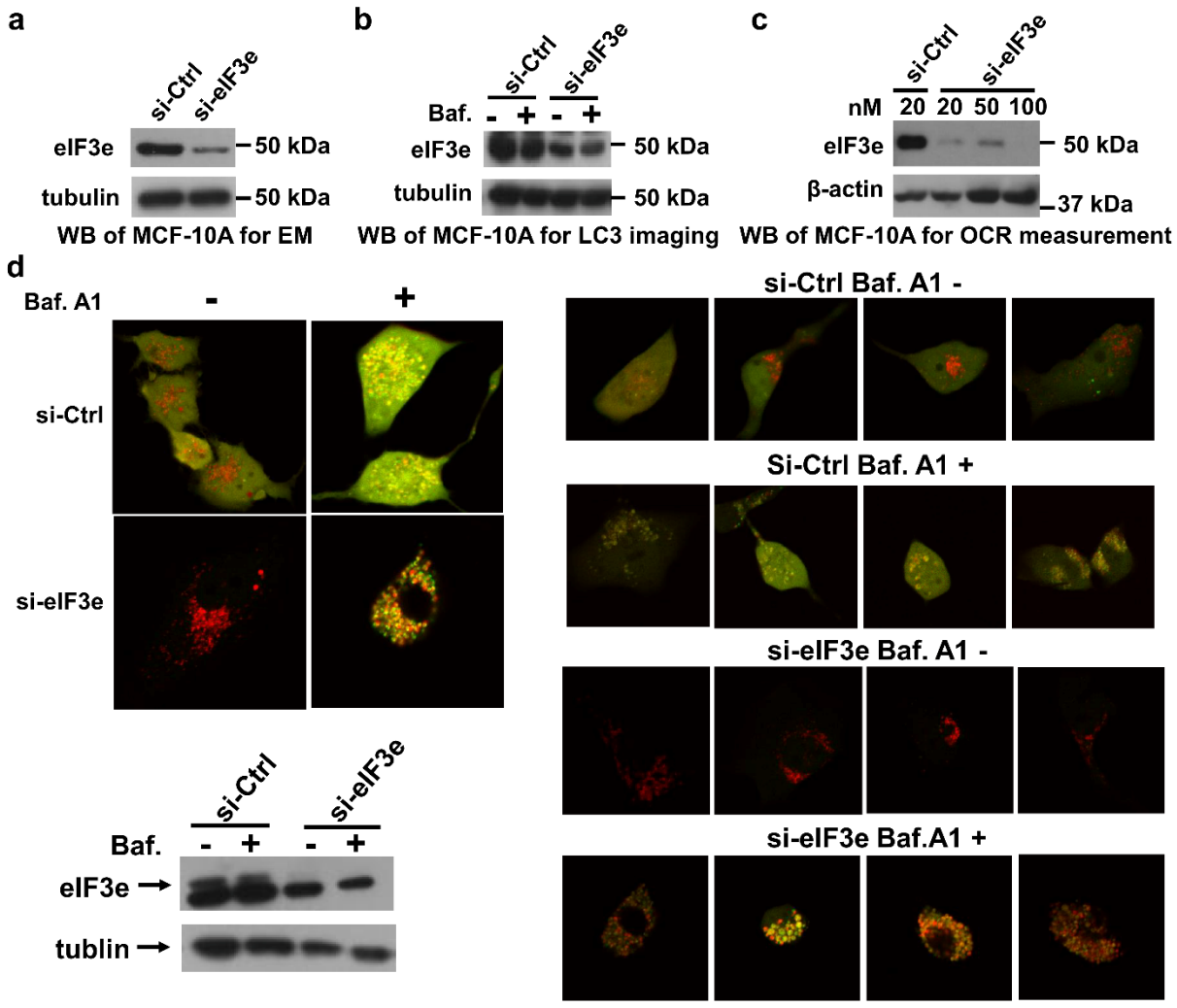

Extended Data Fig. 5 Confirmation of eIF3e knockdown efficiency experiments shown in Fig. 4

a) Immunoblot to confirm the knockdown of eIF3e in MCF-10A cells used for electron microscopy (Fig. 4a).

b) Immunoblot to confirm the knockdown of eIF3e in MCF-10A cells used for live cell imaging of ectopically expressed mCherry-EGFP-LC3B fusion protein (Fig. 4b).

c) Immunoblot to confirm the knockdown of eIF3e in MCF-10A cells used for measurement of oxygen consumption rate (Fig. 4c).

d) Independent repeat of the experiment in Fig. 4b, showing additional examples of si-Control and si-eIF3e cells expressing mCherry-EGFP-LC3B with or without bafilomycin A1 (Baf. A1) treatment. The immunoblot confirms the knockdown of eIF3e in MCF-10A cells used in this experiment.

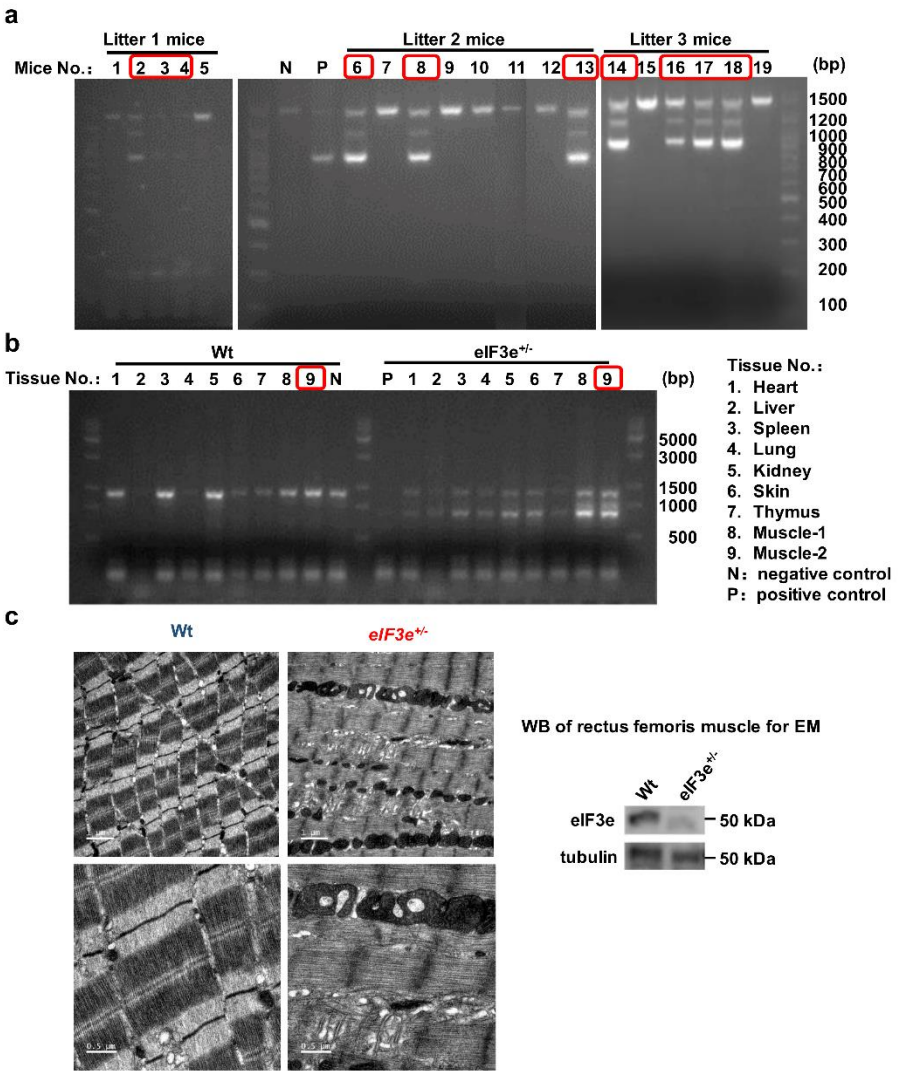

Extended Data Fig. 6 Genotyping of eIF3e$^{+/-}$ mice and muscle phenotype

a) PCR genotyping using tail DNA from three different litters of mice from crosses of eIF3$^{+/-}$ females and males. Heterozygous eIF3$^{+/-}$ mice resulting from the crosses and used in this study are highlighted.

b) PCR genotyping of DNA from the indicated tissues confirms heterozygous knockout of eIF3e. The muscle tissue used for electron microscopy are highlighted.

c) Electron micrographs of rectus femoris muscle from wildtype and eIF3$^{+/-}$ heterozygous knockout mice. The immunoblot confirms the decrease of eIF3e in the muscle tissue shown.

Methods

Tissue culture

MCF-10A cells were cultured in complete growth medium consisting of 50% Dulbecco's modified Eagle's medium and 50% Ham's F12 medium supplemented with 5% fetal bovine serum, 20 ng/mL epidermal growth factor, 10 μg/mL insulin, 5 μg/mL hydrocortisone, 1 unit/mL penicillin, and 1 μg/mL streptomycin under a humified environment with 5% CO_2 at 37°C. Cells were authenticated by short tandem repeat sequencing and determined to be free of mycoplasma.

Knockdown of eIF3e

1×10^7 MCF-10A cells were seeded and grown for 24 hours to a density of ~40%. 10 ∩M control or eIF3e si-RNA were transfected using Lipofectamine 2000 transfection reagent for 72 h before harvesting cells for protein or RNA preparations. The si-RNA oligo sequences were: si-control: 5′-UUCUCCGAACGUGUCACGUdTdT-3′; si-eIF3e: 5′-AAGCUGGCCUCUGAAAUCUUAdTdT-3′ [11].

Western blot

Cells were scraped in 0.1 mL SDS sample buffer (60 mM Tris/Cl, pH 6.8, 5% beta-mercaptoethanol, 2% SDS, 10% glycerol, 0.02% bromophenol blue) followed by heating for 5 min at 95°C. Protein lysates were subjected to SDS-PAGE and transferred onto PVDF membranes. Membranes were blocked in 5% nonfat powdered milk for 1 h at RT and incubated in primary antibodies overnight at 4°C. Membranes were washed 3 times for 10 min each in TBST(10 mM Tris/Cl, pH 7.6, 150 mM NaCl, 1% Tween 20), followed by incubation in goat

anti-mouse or anti-rabbit secondary antibody coupled to horseradish peroxidase for 1 h at RT. Membranes were washed 3 times as above, followed by chemiluminescence detection with ECL reagents. Primary antibodies used were: anti-eIF3a (Novus, cat. NBP1-18891), anti-eIF3b (Bethyl, cat. A301-761A), anti-eIF3d (Bethyl, cat. A301-758A), anti-eIF3e (Bethyl, cat. A302-985A), anti-RPL7 (Abcam, cat. ab72550) and anti-RPS19 (Bethyl, cat. A304-002A).

Sucrose density gradient centrifugation

Total lysate was prepared by scraping 6×10^7 cells into 0.5 ml hypotonic buffer (5 mM Tris-HCl, pH 7.5, 2.5 mM $MgCl_2$, 1.5 mM KCl and 1x protease inhibitor cocktail) supplemented with 100 µg/ml cycloheximide (CHX), 1 mM DTT, and 100 units of RNAse inhibitor. Triton X-100 and sodium deoxycholate were added to a final concentration of 0.5% each, and samples were vortexed for 5 seconds. Samples were centrifuged at 16,000 g for 7 min at 4°C. Supernatants (cytosolic cell extracts) were collected and absorbance at 260 nm was measured. Approximately 10-15 OD_{260}s of lysate was layered over 10% – 50% cold sucrose gradients in buffer (200 mM HEPES-KOH, pH 7.4, 50 mM $MgCl_2$, 1 mM KCl, 100 µg/mL CHX and 1x Pierce™ protease inhibitor). Gradients were centrifuged at 39,000 rpm in a Beckman SW28 rotor for 2 h at 4°C. After centrifugation, 14 equal-sized fractions (0.75 mL/fraction) were collected and analyzed through UV detection. For immunoblotting, fractions were mixed with SDS sample buffer.

Pulsed SILAC sample preparation

MCF-10A cells were grown in DMEM : F12 (SILAC standard) containing light (^{12}C, ^{14}N) lysine and arginine supplemented with 5% dialyzed FBS and EGF, insulin and hydrocortisone as described above for 2 weeks. 1×10^7 cells were treated with eIF3e or control siRNA for 48 h,

followed by changing the light medium to heavy medium containing (^{13}C, ^{15}N) lysine and arginine. Cells were scraped in pre-cooled PBS and pelleted by spinning at 600 g for 5 min at 4 °C. Cell pellets were resuspended in 0.5 mL 8 M urea lysis buffer (8 M urea in 0.2 M Tris/HCl, 4 mM $CaCl_2$, pH 8.0). The supernatant fractions were collected after centrifugation at 12,000 g for 15 min at 4 °C, and protein concentrations were determined by BCA assay (Pierce). Mass spectrometry for the pSILAC analysis was carried out by the National Center for Protein Science Beijing.

Quantitative proteomics of polysomal fractions and purified 80S and eIF3 complexes

MCF-10A cell lysate was fractionated through a 35% sucrose cushion and the polysomal pellet was digested with RNAse I to dissociate polysomes into 80S monosomes. The 80S monosomes were further purified on a 10 – 50% sucrose density gradient. The total cell lysate, the digested polysomes and the 80S monosomes were analyzed by quantitative LC-MS/MS. For analysis of eIF3 complexes, 2 μg of anti-eIF3b antibody were pre-absorbed to 150 μl protein A + G magnetic beads for 2 h at 4 ^{o}C and incubated with gel filtration fractions enriched for eIF3 complexes overnight at 4 ^{o}C. Beads were washed with IP buffer (100 mM Tris, pH 7.5, 150 mM NaCl, 0.5% Triton X-100) 3 times for 5 min each. Following trypsin digestion, peptide mixtures were re-dissolved in 0.1% formic acid in ultrapure water before being analyzed by HPLC coupled to a Q-Exactive mass spectrometer (Thermo Fisher Scientific) operated in positive data-dependent acquisition mode. Protein identification and quantitation were automatically performed by Thermo Proteome Discoverer (PD 1.4.0288) software against UniProt human protein database release 2016_09. Precursor ion mass tolerance was 10 ppm; fragment ion mass tolerance was 0.5 Da. The FDR of protein and peptide was 0.01. The normalized spectrum

abundance factor (NSAF) was calculated by a custom Pearl script. The mass spectrometry data were submitted to PeptideAtlas (PASS01378).

Transmission electron microscopy

Cell pellets after trypsinization corresponding to 1 × 10^7 cells or fresh tissues removed from mice and dissected into pieces of a volume of ~1 mm^3 were washed with sodium cacodylate buffer pre-cooled to 4 ºC (1 mM $CaCl_2$ in 0.1 M sodium cacodylate buffer, pH 7.4) and immersed in pre-cooled fixation buffer (2.5% glutaraldehyde, 2.4% formaldehyde, and 1 mM $CaCl_2$ in 0.1 M sodium cacodylate buffer, pH 7.4). Samples were fixed overnight at 4°C, washed with sodium cacodylate buffer three times and post-fixed in OsO4 (1% OsO4, 0.1% potassium ferrocyanide, 1 mM $CaCl_2$ in 0.1 M sodium cacodylate buffer, pH 7.4) for 1.5 h at 4°C. Samples were dehydrated in 30% and 50% ethanol and stained in 70% uranyl acetate for 4 h, followed by serial dehydration in 70%, 90% and 100% ethanol. Samples were embedded in Spurr's resin, sectioned into 75 nm slices, and stained with lead citrate for 10 min. Images were taken on a Tecnai Spirit BioTwin TEM.

To quantify mitochondrial area in muscle of wildtype and $eIF3e^{+/-}$ mice, TEM micrographs of muscle in the longitudinal orientation at a magnification of ×13,000 were used. Mitochondrial size measurements were obtained using Image J (version 1.42q, National Institutes of Health, Bethesda, MD) by manually tracing only clearly discernible outlines of muscle mitochondria on TEM micrographs.

Autophagic flux assay

1×10^6 MCF-10A cells were simultaneously transfected with 2 μg pDest-mCherry-EGFP-LC3B and with eIF3e or control siRNA for 48 h using Lipofectamine 2000 transfection reagent. Prior to imaging, cells were treated with 0.2 μM bafilomycin A1 for 12 h, washed with Hank's buffer, and live cells were imaged by confocal microscopy (Zeiss Exciter 5).

Measurement of oxygen consumption rate

The Seahorse XFe96 metabolic flux analyzer was used for measuring oxygen consumption rate (OCR). Wells of the utility plate were filled with 200 μL of XF Calibrant and placed at 37 °C at atmospheric CO_2 overnight before seeding 15,000 MCF cells in complete medium. After 12 – 24 hours, cells were washed with 100 μL XF Base medium (Seahorse Bioscience 102353-100) which has been adjusted to pH 7.4 at 37 °C with 0.1M NaOH. 175 μL XF Base medium was added to all 96 wells and the plate was placed at 37 °C in an incubator at atmospheric CO_2 for 60 min. 1 μM oligomycin, 0.5 μM carbonyl cyanide 4-(trifluoromethoxy)phenylhydrazone (FCCP) and 1 μM of AA/rotenone were added to the injection wells and assays were run according to standard instrument protocol.

Grip strength assay

Forelimb grip strength of mice was measured with the Ugo Basile 47200 Grip-Strength Meter. Each mouse was tested five times and the peak force was recorded. Mice were measured at ages of 2, 3, or 4 months as indicated in Figure 4.

Generation of eIF3e knockout mice

eIF3e conditional knock-out mice crossed with FVB-Tg(Ddx4-cre)1Dcas/JNju mice which were purchased from Shanghai Biomodel Organism Science & Technology Development Co., Ltd. to breed eIF3e$^{+/-}$ heterozygous knock-out mice in which exon2 of eIF3e in one of the DNA strand was floxed. And self-cross eIF3e$^{+/-}$ heterozygous knock-out mice to obtain more eIF3e$^{+/-}$ heterozygous knock-out mice. Genotyping was done by PCR using tail DNA as template. Mice tail were lysed in 500 μl lysis buffer (100 mM Tris, pH 8.0, 200 mM NaCl, 0.2% SDS, 5 mM EDTA, and 75 μg/μL PK enzyme) overnight (＞6 h) at 55°C, then centrifuged at 12,000 g for 10 min at RT to recover the supernatant. An equal volume of isopropanol was added followed by gentle shaking and centrifugation at 12,000 g for 10 min at RT. The DNA pellet was dissolved in 50 μl of ddH_2O. eIF3e genotypes were determined by performing PCR using 100 ng purified genomic DNA as a template and the following primers: forward primer (5′-GGTGTGGAGAAGAAGAGAAGGT-3′) and reverse primer (5′-GCAGGGACAAAGAGTGGAACA -3′). All mice were in a C57BL/6J strain background.

Preparation of ribosome footprint libraries

1 x 10^7 MCF-10A cells were lysed with polysome buffer for 10 min on ice, then 16,000 g spin for 10 min at 4° C to recover lysates [23]. After clarification, 5 OD_{260} units of lysates were treated with 450 units of RNaseI (Ambion) for 45 min at RT. Ribosome protected fragments (RPFs) were isolated by chromatography on a Sephacryl S400 spin column (GE, MicroSpin S-400 HR, 27514001) according to manufacturer's instructions. mRNAs and RPFs were isolated with TRIzol reagent. The rRNA removal for total mRNAs and RPFs was done using Ribo-Zero Gold rRNA removal kit (Illumina, cat, MRZG12324). RPFs were size-selected by 15% denaturing

PAGE and cutting out the gel region corresponding to a size of 26 – 34 nucleotides. An oligonucleotide adaptor was ligated to the 3' end of total mRNAs and RPFs, followed by reverse transcription, circularization and PCR amplification. cDNA libraries were quality tested by running on an Agilent 2100 Bioanalyzer and subjected to 50-bp single end sequencing on an Illumina Hiseq 2000 instrument.

Selective ribosome profiling

2 μg of anti-eIF3b antibody were pre-absorbed to 150 μl protein A + G Sepharose beads and beads were blocked in 0.5% BSA for 0.5 hours at 4 ^{o}C. Beads were incubated overnight with RPFs prepared as described above (the RPF material recovered upon Sephacryl S400 chromatoraphy) at 4 ^{o}C. Beads were washed with IP buffer (100 mM Tris, pH 7.5, 150 mM NaCl, 0.5% Triton X-100) 3 times for 5 min each), and associated RNA was isolated with TRIzol reagent. The cDNA library was constructed and sequenced as described above. All RNAseq data were submitted to Gene Expression Omnibus (GSE131074).

Pre-processing of the ribosome profiling and mRNA-seq data

The human reference genome assembly (GRCh38) and the annotation file downloaded from the Ensembl genome browser were used for all analyses. The pre-processing procedure of the ribosome profiling and mRNA-seq data has been described previously [24]. FastQC (http://www.bioinformatics.babraham.ac.uk/projects/fastqc/) was used for quality control and the adaptor sequence (CTGTAGGCACCATCAAT) in the raw reads of both ribosome profiling and mRNA-seq was trimmed using the Cutadapt program. Reads with length between 25-35 nt were used for ribosome profiling analyses. Low-quality reads with Phred quality scores lower than 25

(>75% of bases) were removed using the fastx quality filter (http://hannonlab.cshl.edu/fastx_toolkit/). Then sequence reads originating from rRNAs were identified and discarded by aligning the reads to human rRNA sequences downloaded from GenBank (https://www.ncbi.nlm.nih.gov/genbank/) using Bowtie 1.1.2 with no mismatch allowed. The remaining reads were mapped to the genome using STAR [25] with the following parameters: --runThreadN 8 --outFilterType Normal --outWigType wiggle --outWigStrand Stranded --outWigNorm RPM --alignEndsType EndToEnd --outFilterMismatchNmax 1 --outFilterMultimapNmax 1 --outSAMtype BAM SortedByCoordinate --quantMode TranscriptomeSAM GeneCounts --outSAMattributes All.

The RNA-seq reads for each gene were counted with HTSeq-count in intersection-strict mode and the read counts of RPF were calculated with a custom script written by Xiao [24]. The translation efficiency (TE) of each gene was calculated by dividing the read count of mRNA by that of RPF. All other analyses were performed using custom scripts written with Python 3.6 and R 3.4.3.

Assessment of 3-nt periodicity and offset determination

3-nt periodicity of the RPF reads aligned by their P-sites was used as a strong evidence of activate translation [10]. We used the RiboCode program [26] to assess the 3-nt periodicity of all Ribo-seq samples.

Meta-analysis of ribosome profiling data

The read counts at each codon of the transcripts were calculated using a custom Python script. As for each transcript, the read counts vector is written as:

$$read\_counts_{transi} = [c_1, c_2, \dots, c_{n-1}, c_n] \qquad (1)$$

Where ci is the read count at codon position i in the transcript, and n represents the length of the ORF in unit of codon. The read counts at each position were normalized by the mean value of each read counts vector without the first 30 codons to exclude the accumulated reads around the start codon. For genes with multiple transcript isoforms, only the longest isoform was used when parsing the genome annotation files.

For the metagene analyses at the global scale, transcripts with more than 300 codons were used. Low level transcripts (raw counts fewer than 128 or normalized counts less than 64) were discarded. However, when specifically studying the metagene spectrum between the codons 25 and 75, the transcripts with ORF length longer than 150 codons and RPKM (reads per kilobase per million mapped reads) values larger than 10 were used. After the filtering steps above, all transcripts were lined up and the mean read density at each position was be calculated as:

$$\overrightarrow{read\_density_i} = \frac{\sum_N ci}{N} \qquad (2)$$

Where N is the numbers of transcripts retained, and ci represents the read density at codon i position. Finally, all mean read density at each position formed a vector that was then used for metagene plots with a moving-average method (size of window: 7 codons; step size: 1 codon).

To identify the mRNAs that contributed to the accumulated RPF reads between codons 25 - 75 upon eIF3E knockdown, we implemented a bootstrap-based procedure, which partitioned the range of codons 25 - 75 into 9 windows with 10 codons each (i.e., bin width = 10 codons, step width = 5 codons). Next, the transcripts that have higher (≥ 2-fold) read density in at least one of the 9 windows and are not lower than control in any other window when comparing the si-eIF3E cells to control knockdown cells were extracted and used for further analysis. Finally,

2683 transcripts were identified with ≥ 2-fold accumulation of ribosomes between codons 25 - 75.

Calculation of ribosome polarity scores

To quantify global differences in the position of ribosomes along transcripts, we computed a polarity score for every gene as described previously [27]. The polarity at position i in a gene of length l is defined as follows:

$$p_i = \frac{d_i w_i}{\sum_{i=1}^{l} \mathrm{d}_i} \qquad (3)$$

Where

$$w_i = \frac{2\mathrm{i} - (l+1)}{l-1} \qquad (4)$$

The d_i and w_i represent the ribosome density and normalized distance from the center of a gene at position i respectively. Polarity score for a gene is the total sum of pi at each position. Also, we excluded the first and the last 15 nt of coding sequences from our analyses. mRNAs with more than 64 reads in coding sequences were used for generating the polarity plots.

Data analysis for selective ribosome profiling

Read counts along each transcript were computed as described in the section above (Meta-analysis of ribosome profiling data). Moving-average method was used to obtain read density at each position along a transcript (size of the window: 7 codons; step size: 1 codon). Enrichment ratios were calculated at each position (i.e., RPFs obtained from eIF3b-associated ribosomes over RPFs obtained for all ribosomes). Remaining zeros at some positions were replaced with

the number 1. Transcripts with a global difference in the positioning of eIF3b-associated ribosomes relative to all ribosomes were identified by comparing their polarity scores (see section above). Specifically, an mRNA with a smaller polarity score based on the eIF3-bound RPF density than the score based on RPF density obtained by conventional ribosome profiling (polarity score difference <0) was defined as an "eIF3-80S 5'-enriched mRNA". In total, 2543 such mRNAs were used for meta-analysis. The 5204 mRNAs with a polarity score difference >0 were defined as "eIF3-80S 5'-depleted mRNAs". Only transcripts longer than 150 codons with RPKM in the coding region larger than 10 were used. Meta-analysis for the enrichment ratios was done as described above for conventional ribosome profiling**.**

Hydrophobicity index

Hydrophobicity index (also called hydropathy index) of an amino acid is a number representing the hydrophobic or hydrophilic properties of its sidechain. The hydrophobicity index was download from AAindex (https://www.genome.jp/aaindex/) and the mean values at each position along the amino acid sequences were fed into a vector used for metagene analysis.

Charges of amino acid

Amino acids with positive charges (Lys and Arg) were assigned a score of 1, amino acids with negative charge were assigned a score of -1, and neutral amino acids were assigned a score of 0. Proteins were aligned at the starting methionine and charge scores at each residue were computed and averaged across all proteins in the analysis. Average scores of all proteins were plotted.

The local tAI

The local tAI (tRNA adaptation index) was computed as previously described [28]. That is, let n_i be the number of tRNA isoacceptors recognizing codon i. Let tGCNij be the copy number of the jth tRNA that recognizes the ith codon and let Sij be the selective constraint on the efficiency of the codon-anticodon coupling. The absolute adaptiveness, Wi, for each codon i is

$$W_i = \sum_{j=1}^{n_i} (1 - S_{ij}) tGCN_{ij}. \qquad (5)$$

From the absolute adaptiveness we could get the relative adaptiveness value of codon i, namely wi, by normalizing the Wi values (dividing them by the maximum of all Wi values).

$$w_i = \frac{W_i}{maxW_i} \qquad (6)$$

The classic tAI of a gene later would be calculated as the geometric mean of wi. In the present study, however, we intended to observe the tAI values at each position along transcripts. Therefore, wi was treated as the local tRNA adaptiveness index for codon i, after which all local tAI values of each transcript were lined up and mean values at each position were computed and plotted. The copy numbers of each tRNA were downloaded from GtRNAdb (http://gtrnadb.ucsc.edu/) and the scores Sij for wobble nucleoside-nucleoside pairing were taken from Tuller et al. [28].

Statistical analysis

All p values for the ribosome profiling data were calculated using t-tests based on custom R or Python scripts. Statistical analysis of the remaining datasets was performed with Microsoft

Excel. Typically, data were averaged, standard deviations calculated, and statistical significance was assessed using the T.Test function assuming two-tailed distribution and unequal variance.

Functional pathway analysis

For each given gene list, pathway and process enrichment analysis has been carried out with Metascape (metascape.org [29]) with the following ontology sources: GO Biological Processes, GO Cellular Components, Canonical Pathways and CORUM. All genes in the genome were used as the enrichment background. Terms with a p-value < 0.01, a minimum count of 3, and an enrichment factor > 1.5 (the enrichment factor is the ratio between the observed counts and the counts expected by chance) were collected and grouped into clusters based on their membership similarities. According to the description at metascape.org, p-values were calculated based on the accumulative hypergeometric distribution, and q-values were calculated using the Benjamini-Hochberg procedure to account for multiple testing. To capture relationships between enriched functional terms, a subset was selected and rendered as a network plot, where terms with a similarity > 0.3 were connected by edges. Terms with the best p-values from each of 20 clusters were selected, and the network was downloaded as a Cytoscape [30] file. Each node represents an enriched term colored by its p-value.